UMYU Scientifica, Vol. 5 NO. 1, March 2026, Pp 276 – 283
https://doi.org/10.56919/usci.2651.023
ISSN: 2955 – 1145 (print); 2955 – 1153 (online)
A periodical of the Faculty of Natural and Applied Sciences, UMYU, Katsina

ORIGINAL RESEARCH ARTICLE

Defect-Mediated Cobalt-Doped SnO_2 Nanostructures for Enhanced Visible-Light Photocatalytic Degradation

Danasabe Abdullahi Ibrahim[1,2]*, Adam Usman[2] and Ahmed D. Abubakar[2]
[1]Department of Physics, Nigerian Army University, Biu, Nigeria
[2]Department of Physics, Modibbo Adama University, Yola, Nigeria

ABSTRACT
The development of visible-light-responsive photocatalysts is essential for sustainable wastewater remediation. In this study, defect-engineered cobalt-doped SnO_2 nanostructures were synthesized via a co-precipitation method and evaluated for the photocatalytic degradation of Rhodamine B. X-ray diffraction analysis confirmed the formation of a tetragonal rutile phase, while peak shifts and broadening in the doped sample indicated lattice distortion and reduced crystallite size. X-ray photoelectron spectroscopy revealed the presence of Co^{2+} species, mixed Sn^{4+}/Sn^{2+} oxidation states, and abundant oxygen vacancies, confirming successful defect formation. Under visible-light irradiation, the 2 mol% Co–SnO_2 exhibited significantly enhanced photocatalytic performance, achieving approximately 99% degradation within 300 minutes, compared to ~80% for pristine SnO_2. Kinetic studies showed that the degradation follows pseudo-first-order behavior, with a rate constant of 0.00557 min^{-1} for the doped sample, corresponding to an approximately 2.6-fold improvement. The enhanced activity is attributed to defect-induced charge separation, improved visible-light absorption, and suppressed electron–hole recombination. These results demonstrate that cobalt-induced defect engineering is an effective strategy for enhancing the photocatalytic efficiency of SnO_2 nanostructures for environmental applications.

ARTICLE HISTORY
Received December 17, 2025
Accepted March 12, 2026
Published March 26, 2026

KEYWORDS
SnO_2 nanostructures; cobalt doping; defect engineering; visible-light photocatalysis; Rhodamine B; kinetics

INTRODUCTION
The continuous discharge of organic pollutants from industrial, pharmaceutical, and domestic sources has intensified environmental concerns related to water contamination. These pollutants are often persistent, toxic, and resistant to conventional treatment techniques, thereby necessitating the development of advanced remediation technologies (Zhu and Wang, 2025; Paul and Ahmaruzzaman, 2025). Semiconductor-based photocatalysis has emerged as an efficient and environmentally benign approach for degrading organic contaminants into harmless end products. Among various photocatalysts, tin dioxide (SnO_2) is widely studied due to its chemical stability, non-toxicity, and cost-effectiveness. However, its relatively wide band gap (~3.6 eV) restricts its photocatalytic activity primarily to the ultraviolet region, limiting its utilization under solar irradiation (Imam et al., 2025).

To address this limitation, defect engineering through transition metal doping has been extensively explored. Incorporation of dopants such as cobalt can introduce lattice distortions, oxygen vacancies, and intermediate energy states within the band gap. These modifications enhance visible-light absorption and improve charge carrier separation efficiency (Nuno, et al., 2019; Liang et al., 2025). Cobalt doping is particularly effective due to its ability to substitute Sn^{4+} ions, thereby inducing charge imbalance and promoting oxygen vacancy formation. These defects act as active sites for photocatalytic reactions and facilitate electron–hole separation, leading to improved photocatalytic performance (Dana et al., 2020).

In this study, pure and 2 mol% cobalt-doped SnO_2 nanostructures were synthesized via a co-precipitation method. Their structural, surface, and photocatalytic properties were systematically investigated to elucidate the role of defect engineering in enhancing visible-light-driven photocatalysis.

Correspondence: Danasabe Abdullahi Ibrahim. Department of Physics, Faculty of Natural and Applied Sciences, Nigerian Army University, Biu, Nigeria. ✉ danasabe1.abdullahi1@gmail.com.
How to cite: Ibrahim, D. A., Usman, A. & Abubakar, A. D. (2026). Defect-Mediated Cobalt-Doped SnO_2 Nanostructures for Enhanced Visible-Light Photocatalytic Degradation. *UMYU Scientifica*, 5(1), 276 – 283. https://doi.org/10.56919/usci.2651.023

MATERIALS AND METHODS

Experimental

All chemicals used in this study were of analytical grade and utilized without further purification. Tin(II) chloride dihydrate ($SnCl_2 \cdot 2H_2O$), cobalt(II) chloride hexahydrate ($CoCl_2 \cdot 6H_2O$), sodium hydroxide (NaOH), and Rhodamine B (RhB) dye were obtained from commercial suppliers. Deionized water was used throughout all experimental procedures.

All glassware was thoroughly cleaned, rinsed with deionized water, and dried prior to use. Magnetic stirring was employed to ensure homogeneous mixing during synthesis. All experiments were carried out under ambient laboratory conditions unless otherwise stated.

Synthesis of Pure SnO_2 Nanostructures

Pure SnO_2 nanostructures were synthesized via a co-precipitation method following a modified procedure reported in the literature (Sathiyamurthy, 2020). An aqueous solution of $SnCl_2 \cdot 2H_2O$ (0.1 M) was prepared and stirred continuously at room temperature.

A 1.0 M NaOH solution was added dropwise under constant stirring until the pH of the solution reached approximately 10–11, resulting in the formation of a white precipitate. The reaction mixture was further stirred for 2 h to ensure complete precipitation and then aged for 12 h.

The precipitate was collected by filtration, washed repeatedly with deionized water to remove residual ions, and dried at 80 °C for 12 h. The dried sample was subsequently calcined at 500 °C for 2 h in air to obtain crystalline SnO_2 nanostructures.

Synthesis of Co-Doped SnO_2 Nanostructures

Cobalt-doped SnO_2 nanostructures (2 mol% Co) were synthesized using a similar co-precipitation method. Appropriate stoichiometric amounts of $SnCl_2 \cdot 2H_2O$ and $CoCl_2 \cdot 6H_2O$ were dissolved in deionized water to obtain a homogeneous precursor solution, maintaining a cobalt doping concentration of 2 mol% relative to tin.

The mixed solution was stirred continuously, and 1.0 M NaOH was added dropwise until the pH reached approximately 10–11. The resulting suspension was stirred for 2 h and aged for 12 h to facilitate uniform incorporation of cobalt ions into the SnO_2 lattice.

The precipitate was filtered, washed thoroughly with deionized water, and dried at 80 °C for 12 h. The dried product was then calcined at 500 °C for 2 h to obtain Co-doped SnO_2 nanostructures.

Characterization Techniques

The crystalline structure and phase composition of the synthesized samples were analyzed using X-ray diffraction (XRD). Surface chemical composition and oxidation states were examined using X-ray photoelectron spectroscopy (XPS). Optical properties and photocatalytic performance were evaluated using UV–Visible spectroscopy by monitoring changes in the absorbance of Rhodamine B solution during irradiation.

Photocatalytic Activity Evaluation

The photocatalytic activity of the synthesized samples was evaluated by the degradation of Rhodamine B under visible-light irradiation. A known amount of photocatalyst (50 mg) was dispersed in 100 mL of Rhodamine B solution with an initial concentration of 10 mg L^{-1}.

Before irradiation, the suspension was magnetically stirred in the dark for 30 min to establish adsorption–desorption equilibrium between the dye molecules and the catalyst surface. Subsequently, the reaction mixture was exposed to visible-light irradiation using a 300 W xenon lamp equipped with a UV cut-off filter. The light intensity at the surface of the reaction system was maintained at approximately 100 mW cm^{-2}.

At regular time intervals, aliquots were withdrawn, centrifuged to remove catalyst particles, and analyzed using a UV–Visible spectrophotometer by monitoring the absorbance at ~554 nm.

The degradation efficiency was calculated using:

$$\text{Degradation (\%)} = (1 - \frac{C_t}{C_0}) \times 100$$

where C_0 and C_t represent the initial and time-dependent concentrations of Rhodamine B, respectively.

The photocatalytic kinetics were analyzed using the pseudo-first-order Langmuir–Hinshelwood model (Mills and Le Hunte, 1997; Konstantinou and Albanis, 2004).

RESULTS AND DISCUSSION

Structural Properties (XRD)

X-ray diffraction (XRD) analysis provides detailed insight into the crystallographic structure, phase composition, and crystallite characteristics of the synthesized nanomaterials. The diffraction patterns of pristine SnO_2 and 2 mol% cobalt-doped SnO_2 are presented in Figure 1, illustrating the influence of cobalt incorporation on the crystal structure and lattice properties.

The diffraction patterns of both samples exhibit well-defined peaks that can be indexed to the tetragonal rutile phase of SnO_2. Prominent reflections corresponding to the (110), (101), (200), (111), and (211) planes are clearly observed, confirming the crystalline nature of the synthesized materials. The most intense peak appears around $2\theta \approx 26–27°$, corresponding to the (110) plane, indicating a preferred orientation along this direction. No additional peaks associated with secondary phases such as cobalt oxides are detected, suggesting that cobalt ions are successfully incorporated into the SnO_2 lattice without forming separate crystalline phases. However, a closer examination reveals that the Co-doped sample exhibits slight shifts in peak positions toward higher 2θ values,

accompanied by noticeable peak broadening and a reduction in peak intensity compared to pristine SnO_2.

The observed shift toward higher 2θ values indicates a decrease in lattice spacing, which can be attributed to the substitution of Sn^{4+} ions (ionic radius ≈ 0.69 Å) with smaller Co^{2+} ions (ionic radius ≈ 0.58 Å). This substitution results in lattice contraction and confirms the successful incorporation of cobalt into the SnO_2 crystal structure. The peak broadening observed in the doped sample suggests a reduction in crystallite size and an increase in lattice strain. These features are characteristic of defect formation within the crystal lattice. The introduction of Co^{2+} ions creates charge imbalance, which promotes the formation of oxygen vacancies. These vacancies act as defect sites that modify the electronic structure and enhance photocatalytic activity by facilitating charge separation and providing active sites for surface reactions.

Additionally, the decrease in peak intensity in the Co-doped sample indicates a slight reduction in crystallinity, which is often associated with increased defect density. Such defect-rich structures are beneficial for photocatalytic applications, as they improve adsorption capacity and enhance the interaction between the catalyst surface and pollutant molecules.

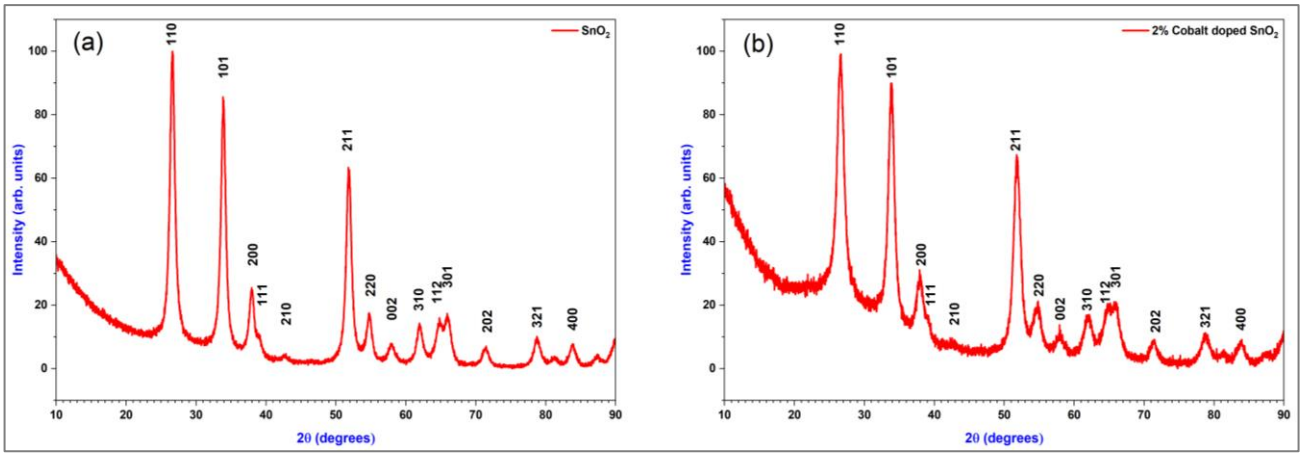

Figure 1: XRD patterns of (a) pure SnO_2 and (b) 2% Co–SnO_2.

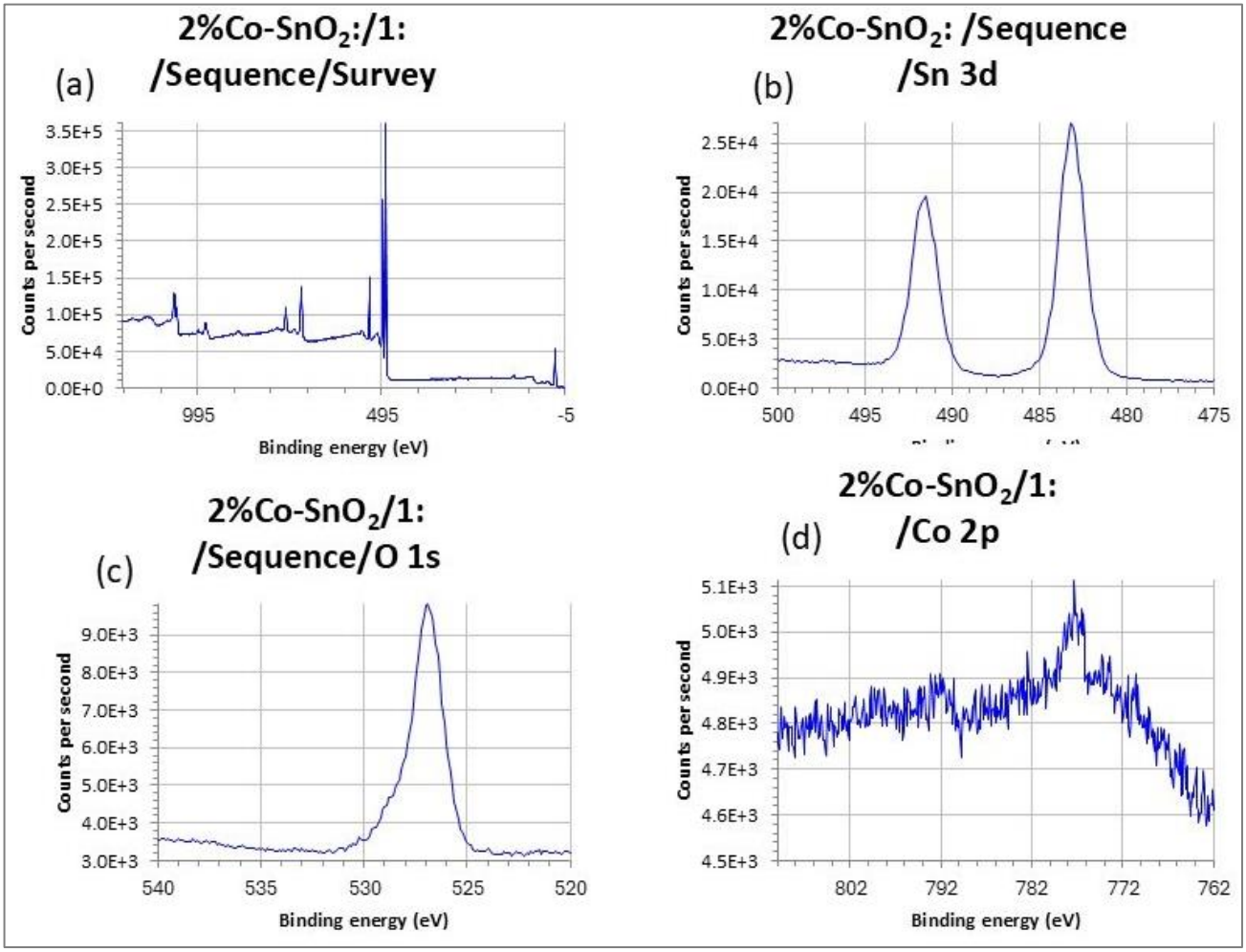

Figure 2: XPS spectra of 2% Co–SnO_2: (a) survey spectrum, (b) Sn 3d, (c) O 1s, and (d) Co 2p.

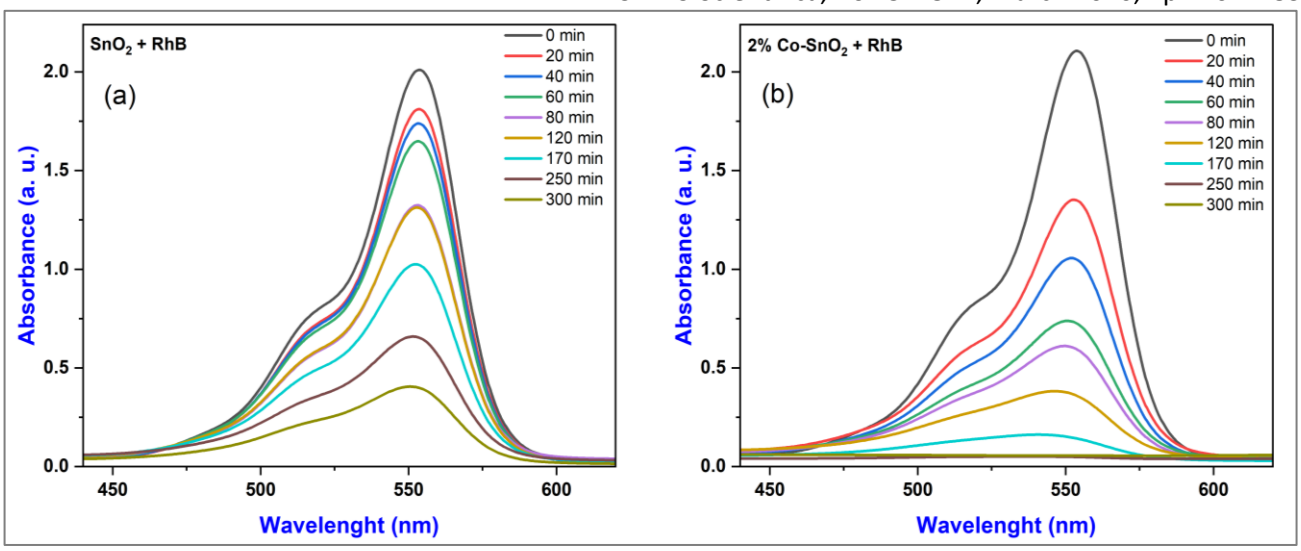

Figure 3: UV–Vis absorption spectra of Rhodamine B degradation over (a) pure SnO_2 and (b) 2% Co–SnO_2 at different irradiation times.

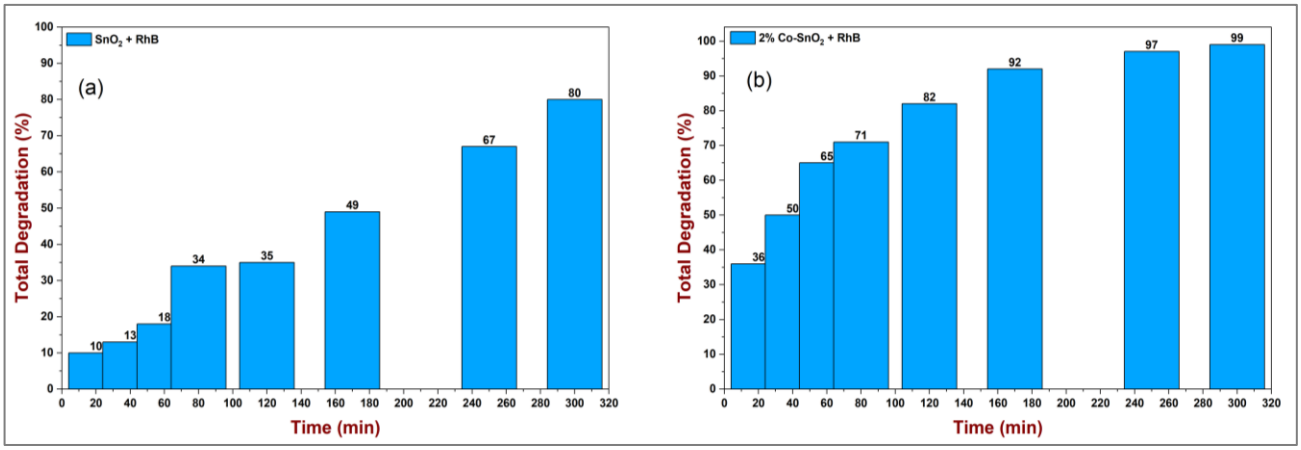

Figure 4: Percentage degradation of Rhodamine B over time using (a) pure SnO_2 and (b) 2% Co–SnO_2.

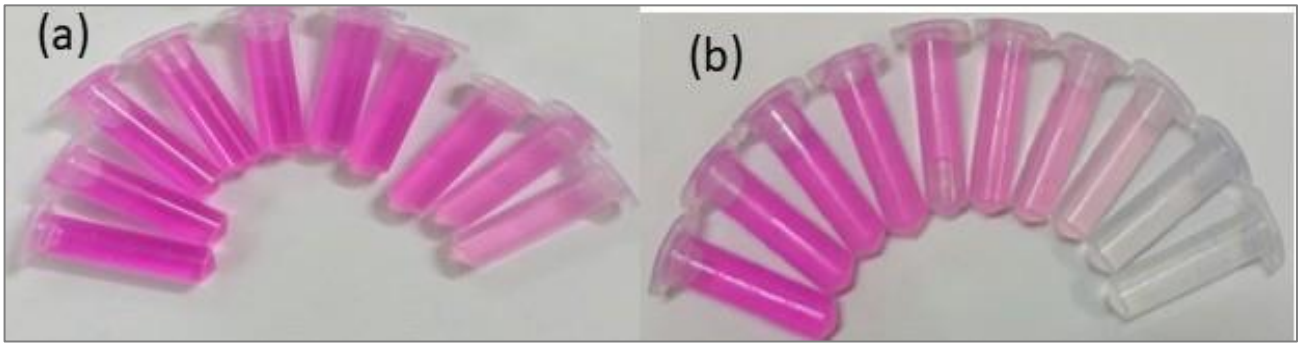

Figure 5: Photographic sequence showing degradation of Rhodamine B using (a) pure SnO_2 and (b) 2% Co–SnO_2.

The structural changes observed in this study are consistent with previous reports on transition metal-doped SnO_2 systems. Nuno, et al. (2019) reported similar peak shifts and broadening effects attributed to dopant incorporation and lattice distortion. Likewise, Dana et al. (2020) demonstrated that cobalt doping induces oxygen vacancies and enhances photocatalytic performance through defect-mediated mechanisms. These findings support the conclusion that cobalt incorporation effectively modifies the structural and electronic properties of SnO_2, thereby improving its photocatalytic efficiency.

Surface Chemical States (XPS Analysis)

X-ray photoelectron spectroscopy (XPS) was employed to investigate the surface chemical composition, oxidation states, and defect structure of the synthesized Co-doped SnO_2 nanostructures. The XPS spectra presented in Figure 2 provide detailed information on elemental composition and the chemical environment of Sn, Co, and O species.

The survey spectrum (Figure 2a) confirms the presence of Sn, O, and Co elements in the doped sample, indicating successful incorporation of cobalt into the SnO_2 matrix

without detectable impurities. The high-resolution Sn 3d spectrum (Figure 2b) exhibits two prominent peaks corresponding to Sn $3d_5/_2$ and Sn $3d_3/_2$, typically located around binding energies of ~486 eV and ~495 eV, respectively. These peaks confirm that tin exists predominantly in the Sn^{4+} oxidation state, which is characteristic of SnO_2. A slight asymmetry or broadening in the peaks suggests the possible presence of a minor Sn^{2+} component.

The O 1s spectrum (Figure 2c) displays a main peak centered around ~529–530 eV, attributed to lattice oxygen (O^{2-}) in SnO_2. A secondary shoulder or broad feature at higher binding energy (~531–532 eV) is observed, which is commonly associated with oxygen vacancies or surface-adsorbed oxygen species. The Co 2p spectrum (Figure 2d) shows characteristic peaks around ~780–782 eV, corresponding to Co $2p_3/_2$, along with possible satellite features. These peaks indicate the presence of Co^{2+} species, confirming that cobalt is incorporated into the SnO_2 lattice rather than forming separate metallic or oxide phases.

The XPS results provide strong evidence for defect formation and successful cobalt doping in the SnO_2 structure. The dominance of Sn^{4+} confirms that the host lattice remains largely intact, while the presence of minor Sn^{2+} suggests partial reduction, which is often associated with oxygen deficiency. The appearance of oxygen vacancy-related peaks in the O 1s spectrum indicates the formation of defect sites within the lattice. These vacancies arise due to charge imbalance when Co^{2+} substitutes for Sn^{4+}, necessitating the removal of oxygen atoms to maintain charge neutrality.

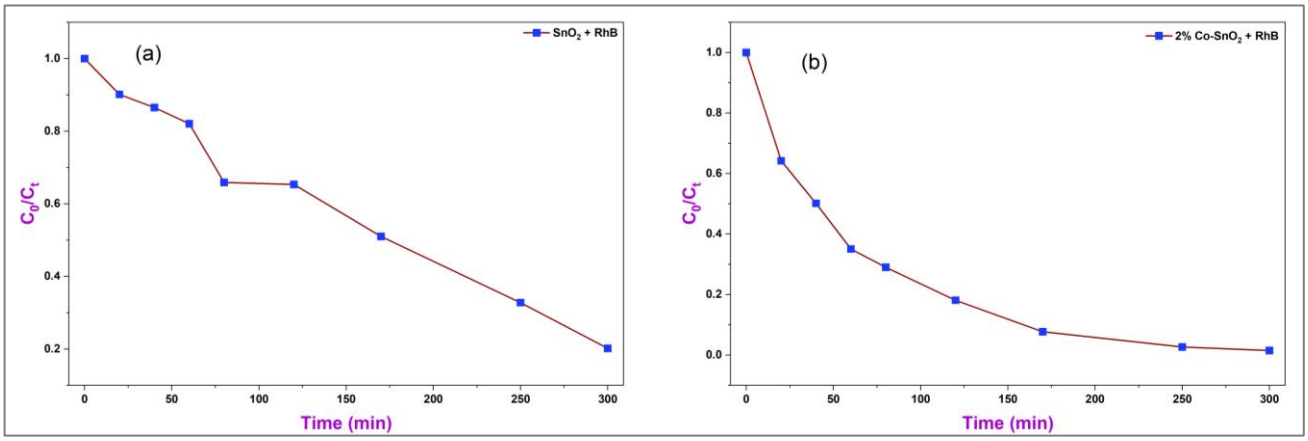

Figure 6: Normalized concentration (C_0/C_t) versus irradiation time for (a) pure SnO_2 and (b) 2% Co–SnO_2.

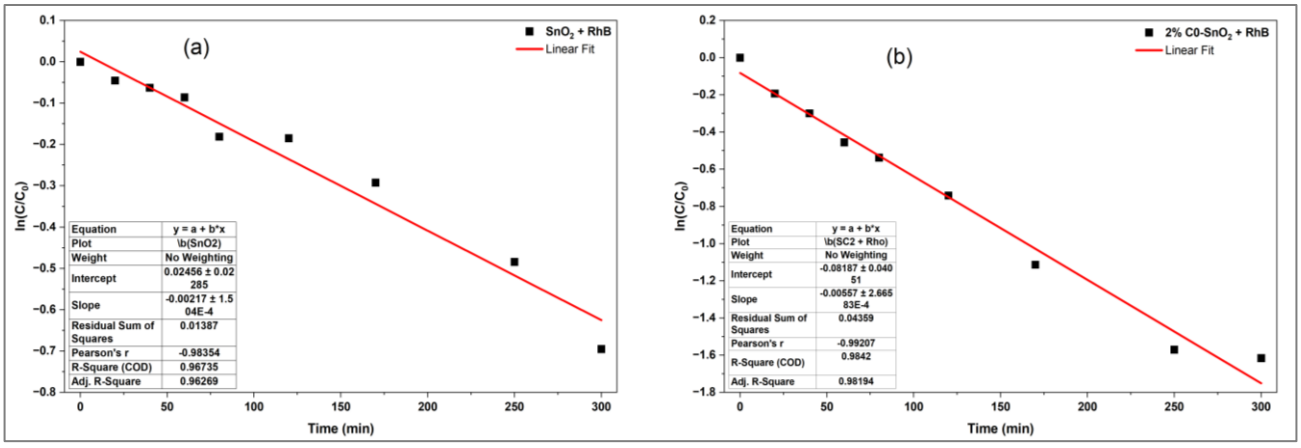

Figure 7: Pseudo-first-order kinetic plots $\ln(C_0/C_t)$ versus time for (a) pure SnO_2 and (b) 2% Co–SnO_2.

The incorporation of Co^{2+} ions introduces localized electronic states within the band structure, which play a crucial role in enhancing visible-light absorption. Furthermore, oxygen vacancies act as trapping centers for photogenerated electrons, thereby reducing electron–hole recombination and prolonging charge carrier lifetime. The combined effect of Co doping and oxygen vacancy formation leads to improved charge separation efficiency and increased availability of reactive oxygen species, which are essential for photocatalytic degradation processes.

The observed XPS features are consistent with previous studies on defect-engineered metal oxide photocatalysts. Imam et al. (2025) reported that oxygen vacancies and mixed oxidation states significantly enhance photocatalytic activity by improving charge carrier dynamics. Similarly, Liang et al. (2025) demonstrated that transition metal doping promotes defect formation and enhances visible-light response in metal oxides. Furthermore, Dana et al. (2020) observed similar Co^{2+} incorporation and oxygen vacancy formation in Co-doped SnO_2 systems, which resulted in improved photocatalytic performance. These findings strongly support the role of defect-mediated electronic modification in enhancing the functional properties of SnO_2 nanostructures.

Photocatalytic Activity (UV–Vis Analysis)

UV–Visible spectroscopy was employed to monitor the photocatalytic degradation of Rhodamine B (RhB) under visible-light irradiation in the presence of pristine SnO_2 and Co-doped SnO_2. The evolution of absorption spectra at different irradiation times is presented in Figure 3, providing insight into the degradation behavior of the dye molecules.

The absorption spectra of RhB exhibit a characteristic peak centered around ~554 nm, corresponding to its chromophoric structure. As irradiation time increases, a gradual decrease in the intensity of this peak is observed for both catalysts, indicating progressive degradation of the dye. However, a more pronounced and rapid reduction in absorbance is observed for the Co-doped SnO_2 sample compared to pristine SnO_2. In the case of pure SnO_2, the absorption peak decreases steadily but remains significant even after extended irradiation. In contrast, the Co-doped sample shows a drastic reduction in peak intensity within shorter irradiation times, approaching near-complete disappearance at prolonged exposure.

Additionally, a slight blue shift in the absorption peak may be observed during degradation, which is indicative of the stepwise de-ethylation process of RhB molecules. The enhanced decrease in absorbance for the Co-doped SnO_2 indicates superior photocatalytic efficiency. This improvement can be attributed to the presence of cobalt-induced defect states and oxygen vacancies, which enhance visible-light absorption and facilitate efficient charge carrier separation.

The introduction of defect levels within the band gap allows for better utilization of visible light, while oxygen vacancies act as trapping sites that reduce electron–hole recombination. As a result, more reactive species such as hydroxyl radicals (•OH) and superoxide radicals ($\bullet O_2^-$) are generated, accelerating the degradation of RhB. The observed spectral changes further suggest that the degradation process involves not only chromophore cleavage but also structural transformation of dye molecules, indicating effective photocatalytic mineralization.

These results are consistent with previous studies on transition metal-doped photocatalysts. Dana et al. (2020) reported enhanced visible-light degradation of organic dyes due to improved charge separation in doped SnO_2 systems. Similarly, Paul and Ahmaruzzaman (2025) highlighted the role of defect states and oxygen vacancies in accelerating photocatalytic degradation processes.

Degradation Efficiency

The degradation efficiency of Rhodamine B as a function of irradiation time is illustrated in Figure 4, enabling a quantitative comparison of photocatalytic performance between pristine and Co-doped SnO_2. The degradation efficiency increases progressively with irradiation time for both samples. However, the Co-doped SnO_2 exhibits significantly higher degradation efficiency at all time intervals. At early stages (20–60 min), the Co-doped sample already demonstrates noticeably higher degradation compared to pure SnO_2. As the reaction progresses, the difference becomes more pronounced. After 300 minutes of irradiation, pristine SnO_2 achieves approximately 80% degradation, whereas Co-doped SnO_2 reaches nearly complete degradation (~99%).

The superior degradation efficiency of Co-doped SnO_2 confirms the effectiveness of defect engineering in enhancing photocatalytic activity. The increased efficiency is attributed to improved light absorption, enhanced charge separation, and increased generation of reactive oxygen species. The presence of oxygen vacancies and dopant-induced energy states facilitates faster electron transfer and reduces recombination losses, thereby accelerating the degradation process. Furthermore, the improved surface properties enhance the adsorption of dye molecules, contributing to higher catalytic efficiency. Similar enhancements in degradation efficiency have been reported in defect-engineered photocatalysts, where transition metal doping significantly improves catalytic performance (Geldasa and Dejene, 2025; Zhu and Wang, 2025).

Photographic Evidence

Visual observation of the degradation process provides qualitative confirmation of photocatalytic performance. The color change of Rhodamine B solution during irradiation is shown in Figure 5. The initial deep pink coloration of RhB gradually fades with irradiation time. For the Co-doped SnO_2 sample, the solution becomes nearly colorless after prolonged irradiation, whereas the solution treated with pristine SnO_2 retains a noticeable pink tint. The rapid discoloration observed in the Co-doped system confirms efficient breakdown of dye molecules and supports the spectroscopic findings. This indicates enhanced catalytic activity and improved interaction between the catalyst and pollutant molecules. Photographic validation of dye degradation has been widely reported as complementary evidence in photocatalytic studies (Paul and Ahmaruzzaman, 2025), confirming the reliability of the observed results.

Kinetic Analysis

The kinetics of Rhodamine B degradation were further evaluated using the Langmuir–Hinshelwood model, which is commonly applied to heterogeneous photocatalytic systems. The normalized concentration (C_0/C_t) as a function of irradiation time is presented in Figure 6, while the corresponding pseudo-first-order kinetic plots of $\ln(C_0/C_t)$ versus time are shown in Figure 7. The normalized concentration plots (Figure 6) show a continuous decrease in C_0/C_t with increasing irradiation time for both samples, confirming progressive degradation of Rhodamine B. However, the Co-doped SnO_2 exhibits a significantly steeper decline compared to pristine SnO_2. For pure SnO_2, the degradation proceeds gradually, with C_0/C_t decreasing from 1.0 to

approximately 0.20 after 300 minutes. In contrast, the Co-doped sample shows a much faster reduction, reaching near-zero concentration ($C_0/C_t \approx 0.01$) within the same irradiation period, indicating almost complete degradation. The kinetic plots (Figure 7) display a linear relationship between $\ln(C_0/C_t)$ and irradiation time for both samples, confirming that the degradation process follows pseudo-first-order kinetics. The linear fitting yields high correlation coefficients ($R^2 \approx 0.96$ for SnO_2 and $R^2 \approx 0.98$ for Co–SnO_2), indicating good agreement with the kinetic model.

The calculated rate constants from the slopes are approximately $k = 0.00217\ min^{-1}$ for pure SnO_2 and $k = 0.00557\ min^{-1}$ for Co–SnO_2. This corresponds to an enhancement factor of about 2.5–2.6 times upon cobalt doping. The significantly higher rate constant observed for Co-doped SnO_2 confirms that cobalt incorporation substantially improves the reaction kinetics of photocatalytic degradation. The enhanced kinetic performance is directly linked to the defect-rich structure introduced by doping. Oxygen vacancies and dopant-induced intermediate energy levels facilitate faster charge transfer and reduce recombination losses, thereby increasing the availability of photogenerated electrons and holes for redox reactions. This results in accelerated formation of reactive oxygen species such as hydroxyl radicals (•OH) and superoxide radicals ($\bullet O_2^-$), which are responsible for dye degradation.

Additionally, the improved adsorption properties of the defect-rich surface enhance interaction between the catalyst and Rhodamine B molecules, further contributing to faster reaction rates. The combined effects of improved charge separation, increased active sites, and enhanced surface interactions lead to superior photocatalytic kinetics. The observed pseudo-first-order behavior is consistent with the Langmuir–Hinshelwood model widely reported for photocatalytic degradation of organic pollutants (Mills and Le Hunte, 1997; Konstantinou and Albanis, 2004). Furthermore, the significant increase in rate constant upon cobalt doping aligns with recent studies on defect-engineered photocatalysts, where transition metal doping enhances reaction kinetics by improving charge carrier dynamics and surface reactivity (Geldasa and Dejene, 2025; Zhu and Wang, 2025).

Defect-Mediated Enhancement Mechanism

Understanding the mechanism responsible for the enhanced photocatalytic activity is essential for optimizing the performance of semiconductor materials. In this study, the improved photocatalytic behavior of Co-doped SnO_2 can be attributed to defect-mediated charge carrier dynamics. The doped sample consistently exhibits superior performance compared to pristine SnO_2 across all photocatalytic evaluations, indicating the significant role of cobalt incorporation.

The introduction of Co^{2+} ions into the SnO_2 lattice leads to the formation of oxygen vacancies and intermediate energy states within the band structure. These defect sites enhance visible-light absorption and facilitate efficient separation of photogenerated electron–hole pairs. As a result, charge recombination is suppressed, allowing more charge carriers to participate in surface redox reactions. Furthermore, the presence of oxygen vacancies promotes the generation of reactive oxygen species, which play a crucial role in the degradation of organic pollutants. This defect-driven enhancement mechanism is consistent with recent reports on transition metal-doped semiconductor photocatalysts, where oxygen vacancies and defect states significantly improve photocatalytic efficiency under visible-light irradiation (Imam et al., 2025; Zhu and Wang, 2025).

CONCLUSIONS

In this study, cobalt-doped SnO_2 nanostructures were successfully synthesized via a co-precipitation method and systematically investigated for visible-light-driven photocatalytic degradation of Rhodamine B. X-ray diffraction analysis confirmed the formation of a tetragonal rutile phase, with peak shifts and broadening indicating lattice distortion and reduced crystallite size due to cobalt incorporation. X-ray photoelectron spectroscopy further revealed the presence of Co^{2+} species, mixed oxidation states of tin, and significant oxygen vacancy formation, confirming successful defect engineering.

Photocatalytic studies demonstrated that Co-doped SnO_2 exhibits markedly enhanced performance compared to pristine SnO_2. The doped sample achieved approximately 99% degradation of Rhodamine B within 300 minutes, whereas pure SnO_2 reached about 80% under identical conditions. Kinetic analysis revealed that the degradation process follows pseudo-first-order behavior, with the rate constant of Co–SnO_2 being approximately 2.5–2.6 times higher than that of the undoped sample.

The improved photocatalytic activity is attributed to defect-mediated mechanisms, including oxygen vacancy formation and dopant-induced electronic states, which enhance visible-light absorption, promote efficient charge separation, and suppress electron–hole recombination. These effects lead to increased generation of reactive oxygen species responsible for pollutant degradation. Overall, this study demonstrates that cobalt-induced defect engineering is an effective strategy for enhancing the photocatalytic efficiency of SnO_2 nanostructures. The findings highlight the potential of doped metal oxide systems for practical applications in environmental remediation and wastewater treatment under visible-light irradiation.

REFERENCES

Cullity, B.D. and Stock, S.R., 2001. *Elements of X-ray Diffraction*. 3rd ed. New Jersey: Prentice Hall.

Dana, T., Adriana, P., Maria, S., Teofil, Danut, S., Ramona, C. S., Lucian, B., and Ovidiu, P., 2020. Enhanced photocatalytic activity of Co doped SnO2 nanoparticles by controlling the oxygen vacancy states. Journal of Optical Materials, 110, p.110472. [Crossref]

Fujishima, A., Zhang, X. and Tryk, D.A., 2008. TiO_2 photocatalysis and related surface phenomena. *Surface Science Reports*, 63(12), pp.515–582. [Crossref]

Geldasa, F.T. and Dejene, F.B., 2025. Transition metal doping effects on the structural, mechanical, electronic, and optical properties of α-NiS for photocatalysis applications via DFT + U insights. Journal of Appl. Phys. A, 131, p.869. [Crossref]

Hoffmann, M.R., Martin, S.T., Choi, W. and Bahnemann, D.W., 1995. Environmental applications of semiconductor photocatalysis. *Chemical Reviews*, 95(1), pp.69–96. [Crossref]

Imam, H., Ayesha, B., Imad, K. K. M., Tong, Z., Rashid, K., Zahid, H., Fu-Gen, Y., Chen, Z. Z. and Kamran, K. M., 2025. Advancing environmental remediation: Mechanistic insights into SnO_2-based photocatalysts for organic pollutant degradation and microbial inactivation. Journal of Water Process Engineering, 77, p.108511. [Crossref]

Konstantinou, I.K. and Albanis, T.A., 2004. TiO_2-assisted photocatalytic degradation of azo dyes in aqueous solution: kinetic and mechanistic investigations. *Applied Catalysis B: Environmental*, 49(1), pp.1–14. [Crossref]

Liang, M., Qinran, L., Qingao, Z., Wenqiang D., Yulong, Z., Yuzhen, S. and Xiaoyan C., 2025. Enhanced carrier separation and decreased reaction barrier in cobalt-doped CdIn2S4 nanosheets for photocatalytic hydrogen evolution. Journal of Colloid and Interface Science, 685, pp.1122-1130. [Crossref]

Mills, A. and Le Hunte, S., 1997. An overview of semiconductor photocatalysis. *Journal of Photochemistry and Photobiology A: Chemistry*, 108(1), pp.1–35. [Crossref]

Nuno, P. F. G., Maria, C. P., Paolo A., Erik, C. and Paola C., 2019. The effect of cobalt doping on the efficiency of semiconductor oxides in the photocatalytic water remediation. Journal of Environmental Chemical Engineering, 7(6), p.103475. [Crossref]

Paul, R.K. and Ahmaruzzaman, M., 2025. Advanced photocatalytic degradation of organic pollutants using nanocomposites: mechanisms and applications. *RSC Advances*, 15(38), pp.31313–31359. [Crossref]

Sathiyamurthy, K., 2020. Synthesis of pure SnO2 nanospheres by the co-precipitation method. Malaya Journal of Matematik, 5(2), pp.1247-1250. [Crossref]

Zhu, C. and Wang, X., 2025. Nanomaterial ZnO synthesis and its photocatalytic applications: A review. *Nanomaterials*, 15(9), p.682. [Crossref]